geosciences

MDPI

Article

The Role of Climate: 71 ka of Atmospheric Mercury Deposition in the Southern Hemisphere Recorded by Rano Aroi Mire, Easter Island (Chile)

Marta Pérez-Rodríguez [1,2,*], Olga Margalef [3,4], Juan Pablo Corella [5], Alfonso Saiz-Lopez [5], Sergi Pla-Rabes [4], Santiago Giralt [6] and Antonio Martínez Cortizas [2]

1 Institut für Geoökologie, Abt. Umweltgeochemie, Technische Universität Braunschweig, Langer Kamp, 38106 Braunschweig, Germany
2 Departamento de Edafoloxía e Química Agrícola, Universidade de Santiago de Compostela, 15782 Santiago de Compostela, Spain; antonio.martinez.cortizas@usc.es
3 Spanish National Research Council (CSIC), Global Ecology Unit CREAF-CEAB-UAB, Cerdanyola del Vallès, 08193 Catalonia, Spain; omargalefgeo@gmail.com
4 Ecological Research Center and Forestry Applications (CREAF), Campus de Bellaterra (UAB), Cerdanyola del Vallès, 08193 Barcelona, Spain; sergiplarabes@gmail.com
5 Department of Atmospheric Chemistry and Climate, Institute of Physical Chemistry Rocasolano, Spanish National Research Council (CSIC), Serrano 119, 28006 Madrid, Spain; pablo.corella@mncn.csic.es (J.P.C.); a.saiz@csic.es (A.S.-L.)
6 Institute of Earth Sciences Jaume Almera (ICTJA-CSIC), Lluis Sole i Sabaris s/n, 08028 Barcelona, Spain; sgiralt@ictja.csic.es
* Correspondence: m.perez-rodriguez@tu-bs.de; Tel.: +49-(0)-531-391-7242

Received: 27 August 2018; Accepted: 7 October 2018; Published: 11 October 2018

Abstract: The study of mercury accumulation in peat cores provides an excellent opportunity to improve the knowledge on mercury cycling and depositional processes at remote locations far from pollution sources. We analyzed mercury concentrations in 150 peat samples from two cores from Rano Aroi (Easter Island, 27° S) and in selected vegetation samples of present-day flora of the island, in order to characterize the mercury cycling for the last ~71 ka BP. The mercury concentrations showed values ranging between 35 and 200 ng g^{-1}, except for a large maxima (~1000 ng g^{-1}) which occurred at the end of the Last Glacial Maximum (LGM, ~20 ka cal BP) in both peat cores. Low temperatures during the LGM would accelerate the atmospheric oxidation of Hg(0) to divalent mercury that, coupled with higher rainfall during this period, most likely resulted in a very efficient surface deposition of atmospheric mercury. Two exceptional short-lived Hg peaks occurred during the Holocene at 8.5 (350 ng g^{-1}) and 4.7 (1000 ng g^{-1}) ka cal BP. These values are higher than those recorded in most peat records belonging to the industrial period, highlighting that natural factors played a significant role in Hg accumulation—sometimes even more so than anthropogenic sources. Our results suggest that wet deposition, linked to atmospheric oxidation, was the main process controlling the short-lived Hg events, both in the mire and in the catchment soils.

Keywords: mercury cycle; Easter Island; Pleistocene; Holocene; climate; peatland

1. Introduction

Mercury (Hg) is a metal of environmental concern due to its high volatility, long atmospheric residence time (1–2 years), and the bioaccumulation of its methylated forms. It is released and dispersed in the atmosphere by natural emission sources such as volcanoes, geothermal vents, and Hg-enriched soil, as well as by anthropogenic activities such as mining, coal-fired plants, and chlor-alkali plants [1–3]. Its transport and deposition in different environments on Earth depends on the type of Hg.

Gaseous elemental mercury (Hg(0)) is the dominant form of atmospheric Hg, and it is efficiently transported around the globe by long-range atmospheric transport. It can be oxidized into highly reactive and water soluble divalent species (Hg(II)), and/or particle-bound Hg (Hg(p)) that can be deposited through wet and dry processes onto surfaces. Therefore, atmospheric oxidation of Hg(0) to divalent Hg enhances its deposition to environmental surfaces [1,4,5]. Particle-bound Hg (Hg_p) represents a minor fraction of total Hg in the atmosphere and can be dispersed over tens to hundreds of kilometers [1].

Natural archives such as mires, lake sediments, glacial ice, and marine sediments have been widely used to reconstruct Hg accumulation at the local, regional and global scale [6–10]. These archives have allowed for the identification of processes and factors that control the deposition and accumulation of Hg over time. Most recently, a factor between a three and five-fold increase in the accumulation of Hg was observed in different parts of the world since the Industrial Revolution, suggesting a worldwide increase in atmospheric Hg deposition [6,10,11]. This anthropogenic input overlaps the signal driven by natural processes of deposition and accumulation. Organic matter degradation and mass loss related to peat evolution enhance Hg accumulation in peatlands [12,13]. Short- and long-term climate oscillations seem to play an important role in Hg cycling through (i) controlling the re-emission of some of the accumulated Hg [14]; (ii) inducing Hg depletion events in polar environments during glacial periods [15]; (iii) producing algal or diatom scavenging in lakes or marine environments [10,16–18] or by (iv) releasing Hg from permafrost mires in warm periods [19]. Finally, processes such as volcanism and fires may play a role in releasing Hg into the atmosphere or in the landscape, but the effects are only visible in very specific cases [20–24].

Nevertheless, most of these considerations are almost exclusively based on Holocene records, and only a few studies extend their conclusions back to the Pleistocene. In contrast to the Northern Hemisphere, there is a limited amount of quite heterogeneous information available for the Southern Hemisphere. The works focused on Hg reconstruction in the South Hemisphere are almost exclusively from the Patagonian area. Most of these studies are based on lake sediments [20,21,25,26] and a few on peat [12,27]. More recently, a lacustrine record from NE Brazil has shown the climate influence driving Hg accumulation rates during the past 20,000 years [28].

In a recent work, we studied Hg accumulation in Pinheiros (18° S, 43° W) [29], a Pleistocene age (last ~57 ka) tropical mire located in a valley in Serra do Espinhaço Meridional (state of Minas Gerais, Brazil). In this work, we found that three of the four main processes controlling Hg concentration depended on climate: wet and dry Hg deposition (rainfall and dustfall, respectively), as well as local catchment soil erosion owing to precipitation events [29]. The effect of long-term peat decomposition, the only autogenic process identified, was confined to the Holocene section of the peat [29].

Although some of the mentioned works provided information from Pleistocene sections (~11.2, 14.6, ~57 and 20 cal BP, [12,27–30]), more long-term records from a wider geographical area are needed in order to fully understand the various processes that can influence emission, deposition, and accumulation of Hg in continental ecosystems. In particular, the role of climate through controls on both deposition and accumulation is one of the major issues that needs to be addressed.

In this study, we analyzed two peat cores from Rano Aroi (ARO), a small mire located in Easter Island, which covers the last ~71 ka BP. We determined the Hg content in the peat samples and in selected vegetation samples of present-day flora located in the watershed. Data from two previous studies on the same records [31,32] were used to reconstruct the environment in Rano Aroi between ca. 71.0 ka BP and ca. 9.0 ka cal BP in the ARO 06 01 core, and the last ca. 39.0 ka cal BP in the ARO 08 02 core. Thus, PC1 and PC2 from a Principal Component Analysis (PCA) performed in ARO 06 01 represent the long-term background fluxes of inorganic particulate material and the delivery of large amounts of terrigenous particles transported during wet events, respectively [32]. Nitrogen concentration (TN) and the C/N ratio were used to attribute the contribution of the organic matter source; for example, algae or terrestrial and aquatic plants [32]. Isotopic organic matter data, $\delta^{13}C$ (‰), was used to indicate the C_3 and C_4 vegetation dominance and thus the main climatic conditions. The

objectives of the present research were (i) to reconstruct the Pleistocene Hg flux variability at millennial to centennial resolution and (ii) to determine the main factors that controlled peat Hg concentrations over long time scales.

2. Materials and Methods

2.1. Regional Setting

Easter Island (27°07′ S, 109°22′ W) is a Chilean volcanic island, Miocene in age, located in the southern Pacific Ocean. The nearest continental point from the South American continent lies 3512 km away. The island has a triangular shape and the topography is characterized by more than 70 volcano craters and the rolling surfaces of lava flows [33–35]. The climate is humid subtropical, with average monthly temperatures between 18 °C (August) and 24 °C (February) [36] and highly variable annual rainfall ranging from 500–1800 mm (mean of 1130 mm).

Rano Aroi is a small mire located in an ancient Pleistocene volcano crater close to the most elevated area of the island (27° S, 108° W, 430 m elevation, 0.13 km^2; Figure 1). The crater slopes form a small catchment area (0.158 km^2, maximum dimension 0.21 km North to South). The watershed lithology mainly consists of very porphyritic olivinic tholeite, basalt and hawaiite lava flows, which are rich in iron [34]. The mire is covered by *Scirpus californicus*, *Polygonum acuminatum*, *Asplenium polyodon var. squamulosum*, *Vittaria elongata* and *Cyclosorus interruptus* [37], while the catchment area is covered by grassland and planted eucalyptus. There is a small ravine acting as a natural outflow that infiltrates before reaching the coast. An artificial outlet built in the 1960s has been used to control the maximum outflow from the peatland since then.

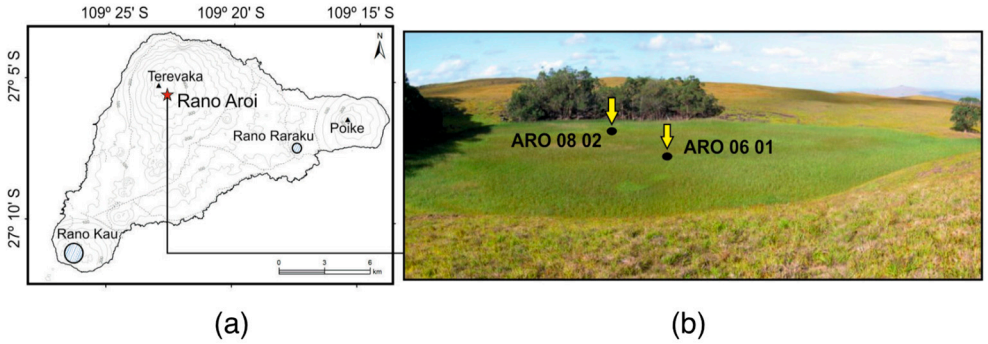

Figure 1. (**a**) Map showing the location of Rano Aroi on the island. (**b**) Photo of the Rano Aroi mire, indicating the location of the studied cores (ARO 06 01, center of the mire and ARO 08 02, margins of the mire).

2.2. Sampling

Two sediment cores (ARO 06 01, 13.9 m long and ARO 08 02, 4 m long) were retrieved from Rano Aroi on March 2006 and October 2008, respectively. The core ARO 06 01 was sampled with a UWITEC corer from the central part of the mire, and the ARO 08 02 with a Russian corer.

The uppermost two meters of the core ARO 06 01 were rejected at the field to avoid potential anthropic remobilization, as described in previous studies [31,32]. Meanwhile, ARO 08 02 was retrieved with a Russian corer from the eastern boundary in order to recover the previously discarded sediments, since the mire's margins were potentially not affected by recent human activities [38,39]. None of the cores retrieved in either campaign reached the bedrock. The cores were sealed, transported to a core repository, and stored in a cold room at +4 °C until sampling. Both cores were lithologically described and sampled for smear slides every 5 cm [31].

2.3. Age Model

The chronology for both cores was fully described by Margalef, et al. [31]. A total of 27 AMS ^{14}C dates were obtained from pollen concentrates of the ARO 06 01 and ARO 02 08 cores in the Poznan Radiocarbon Laboratory (Poland). Only 18 dates were used for the age-depth model. The AMS ages were calibrated using CALIB 6.02 software, and the INTCAL 98 curve [40] and CalPal [41] for samples older than 20,000 radiocarbon year BP. The age model was built by simple linear interpolation [31].

2.4. Geochemical Analysis

Both cores were sampled every 5 cm (286 samples) for total carbon and nitrogen (TC and TN) and stable isotope ($\delta^{13}C$) analyses. Samples were dried at 60 °C for 48 h, frozen with liquid nitrogen, and ground in a ring mill. Analyses were performed using a Finnigan delta Plus EA-CF-IRMS spectrometer, located at the Centres Tècnics i Tecnològics of the Universitat de Barcelona (CCiTUB) [31].

Mercury concentrations were determined in 150 samples of the two cores collected in Rano Aroi and in selected vegetation samples of present-day flora located in the island. Dried, milled samples were analysed for Hg using a Milestone DMA-80 analyser hosted at the Departamento de Bioloxía Funcional (University of Santiago de Compostela). The analysis of one in every five samples was undertaken in duplicate to judge precision. A standard reference material of the moss *Pleurozium schreberi* [42] M3 was run with each set of samples. The quantification limit [average of the blanks + (10 × standard deviation of the blanks)] was 1.34 ng g^{-1}, and the mean recovery of the reference material was 90 ± 4%.

3. Results

3.1. Organic Fraction: Total Carbon, Total Nitrogen, C/N and $\delta^{13}C$

The Rano Aroi deposits are mostly organic, with TC concentrations between 40% and 70% [31]. Total N levels of core ARO 06 01 vary between 0.4% and 2%, with C/N ratios ranging from 40–110 (Figure 2). ARO 08 02 shows similar values with respect to TC (50–60%), TN (0.8–2%, peaking to 2.5% at 140 and 80 cm) and C/N (20–80, with a marked decrease from 2 m upward) (Figure 3).

In ARO 06 01, $\delta^{13}C$ shows a constant value around −14‰ from depths of 14 m to 9 m, whereas from 9 m to 6 m, $\delta^{13}C$ values gradually shift from −14‰ to −26‰ (Figure 2). In the upper five meters, $\delta^{13}C$ values vary around −26‰. In ARO 08 02, a gentle shift of $\delta^{13}C$ from −19‰ to −23‰ occurs from depths of 4 m to 3.5 m (Figure 3). $\delta^{13}C$ curves show high-frequency changes (dips) within the long-term trend [31].

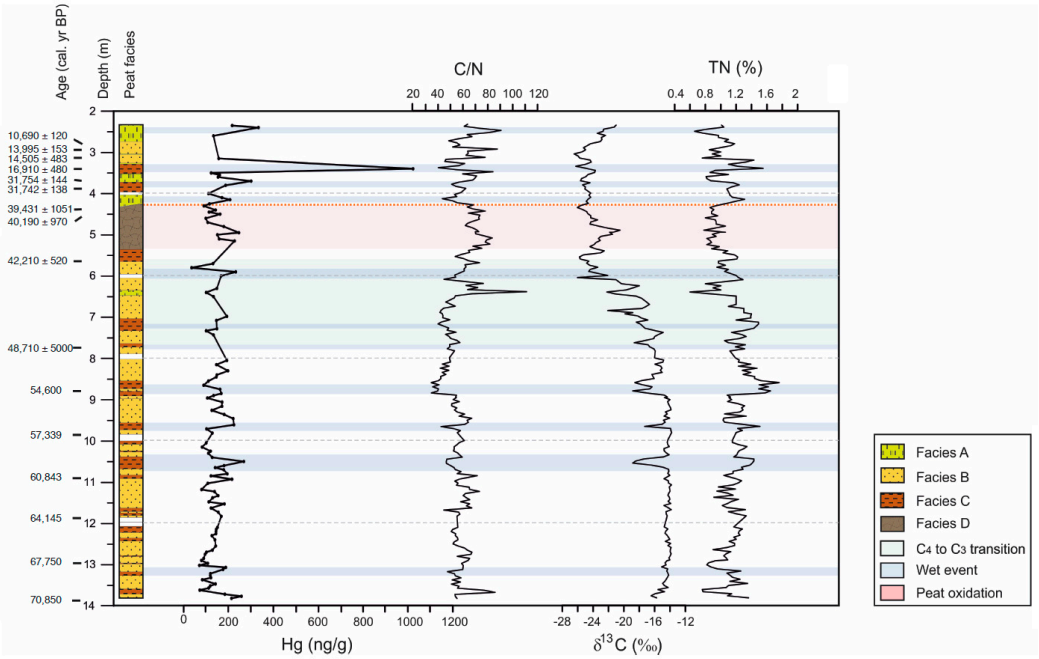

Figure 2. Depth profiles of the main paleoenvironmental proxies and Hg concentration analyzed in the ARO 06 01 core. Lithology and radiocarbon age samples are indicated in the column. Geochemical proxies: total nitrogen and total carbon (TN, C/N) ratios and $\delta^{13}C$, are indicative of the origin of organic matter; and $\delta^{13}C$ (‰) and Facies C [31] are wet event indicators. Periods of wet events and drought conditions are marked.

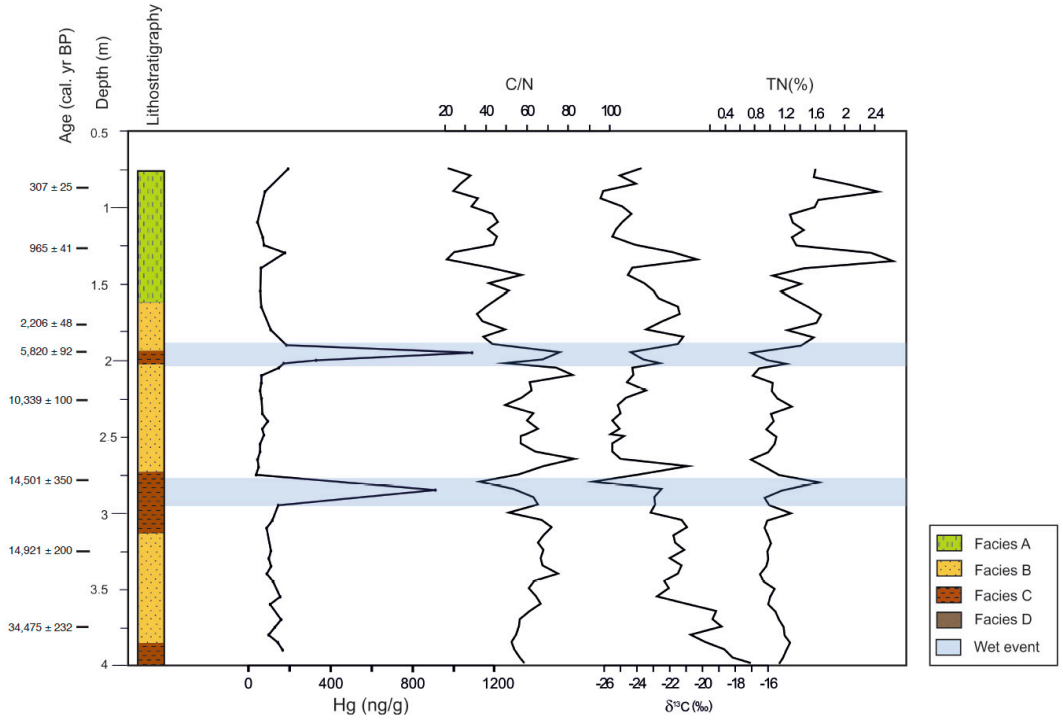

Figure 3. Depth profiles of the main paleoenvironmental proxies and Hg concentration analyzed in the ARO 08 02 core versus depth. Lithology and radiocarbon age samples are indicated in the column. Geochemical proxies: TN (C/N ratios and $\delta^{13}C$, are indicative of the origin of organic matter; Facies C [31] is wet event indicator. Periods of high rainfall events and drought conditions are marked.

3.2. Mercury

Mercury concentrations in the Rano Aroi samples varied in the same range for both cores (Figures 2 and 3). Core ARO 06 08 has values that range between 35 and 1023 ng g^{-1} (147 ± 49, mean ± standard deviation), with the maximum concentration in the sample at 370 cm of core depth. The Hg minimum is located at 580 cm (Figure 2). Core ARO 08 02 displays Hg values that range between 37 and 1088 ng g^{-1} (104 ± 56 ng g^{-1}), and two maxima (1088 and 910 ng g^{-1}) are located at 195 and 285 cm of core depth. According to Hg concentrations, this profile shows three distinct sections: (i) from the base of the core to 290 cm, values increase with depth but with small oscillations (122 ± 26 ng g^{-1}); (ii) from 280 to 202 cm, values are low and almost constant (73 ± 14 ng g^{-1}); and (iii) the upper 190 cm have intermediate values (101 ± 56 ng g^{-1}), with two relative maxima of 177 and 192 ng g^{-1} at 130 and 75 cm, respectively (Figure 3).

Mercury in the vegetation samples had a large concentration range (Table 1). The lowest value (341 ng g^{-1}) corresponds to the rhizome of *Scirpus californicus* and the maximum value (11,175 ng g^{-1}) to an unidentified *rush* sample.

Table 1. Mercury concentrations in vegetation samples collected in Easter Island.

Local/English Name	Scientific Name	Hg (ng g^{-1})
Kikuyu/Kikuyu grass	*Pennisetum clandestinum*	1945
Nga'atu/Totora (duster)	*Scirpus californicus* (duster)	1804
Nga'atu/Totora (rhizome)	*Scirpus californicus* (rhizome)	341
/Rush	no identified	11,175
Maku Piro/molassesgrass	*Melinis minutiflora*	1470

4. Discussion

4.1. Mercury Concentrations in Rano Aroi Records

The two Rano Aroi records (ARO 08 02 and ARO 06 01) cover different temporal ranges (38.7 ka cal BP-present day and 71 ka BP–8.5 ka cal BP, respectively) and were retrieved less than 50 m apart (Figure 1). Previous studies using multiple short cores from the same peatland showed that spatial variability can be a problem for an accurate Hg study, since vegetation and micro-topography changes can affect the interception and retention of atmospheric deposition over relatively short timescales [43,44]. However, the short distance between the cores, the small size of the mire (0.13 km^2), and the age-depth model based on both cores [31] seem to have largely solved this problem. Therefore, we discuss the processes that controlled Hg concentrations in Rano Aroi using both cores together; the differences between them are illustrated based on other proxies (as TC, TN and $\delta^{13}C$).

To the best of our knowledge, there is only one comparable record—the Pleistocene peat record from a tropical-sub tropical area—to Rano Aroi in the literature. This is the Pinheiros mire, located in Minas Gerais state, Brazil. The range of Hg concentrations in Rano Aroi records (~35 and 333 ng g^{-1}) is, in general, comparable with that of Pinheiros mire (~36–370 ng g^{-1}) [29], although the minima found in the Brazilian mire are considerably lower than those in Rano Aroi (<2 vs. 35 ng g^{-1}), probably due to the large quartz content of the corresponding peat sections in the former [29]. On the other hand, the ARO cores show two extraordinary Hg peaks of ~1000 ng g^{-1} at ~20.0 ka cal BP and ~4.7 ka cal BP (Figures 4 and 5) that are more than two-fold the maximum found in the Brazilian record.

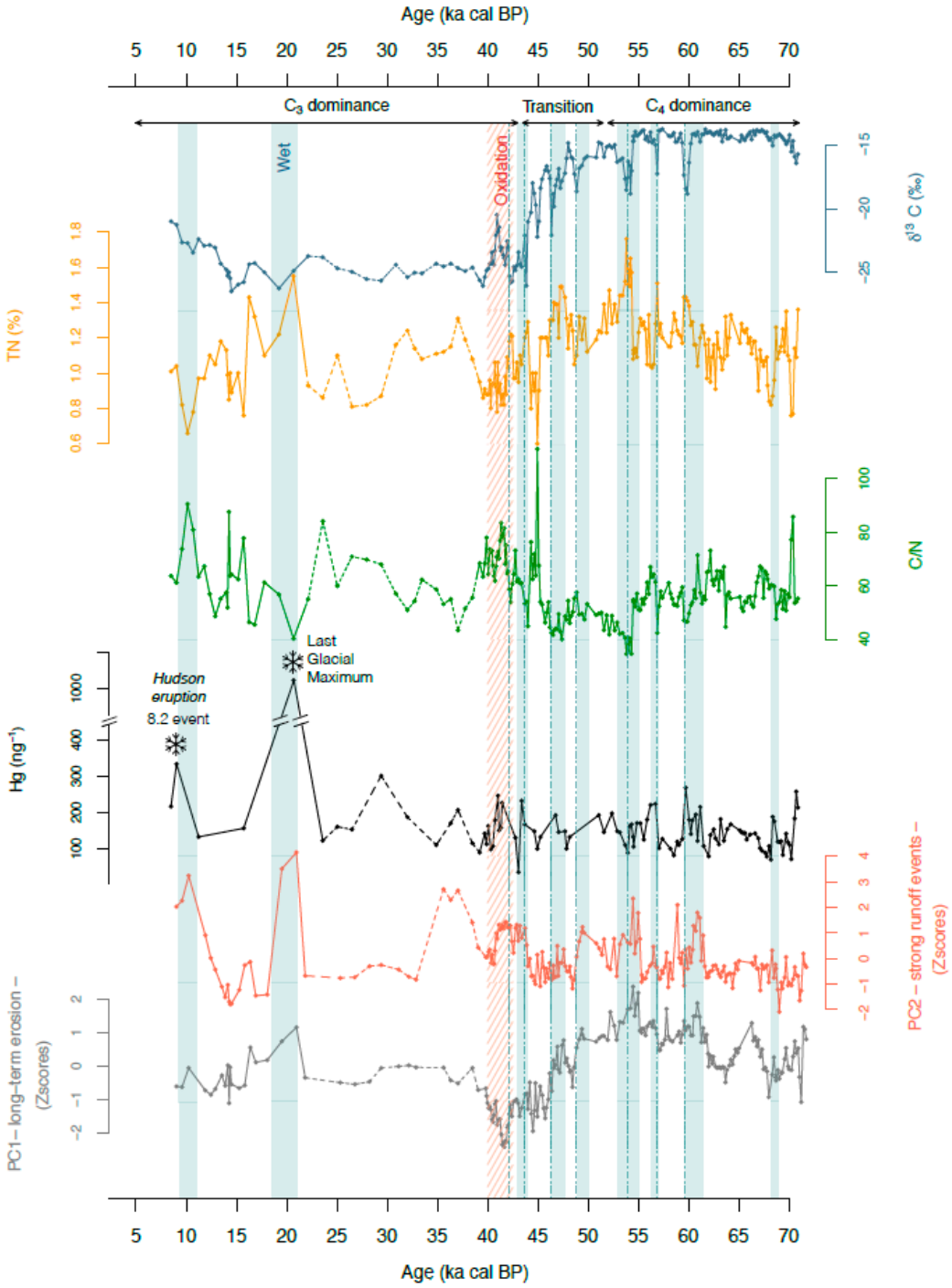

Figure 4. Mercury concentration and main proxies; from bottom to top: PC1, PC2, Hg concentration, C/N, TN and $\delta^{13}C$ used to reconstruct the environment in Rano Aroi between ca. 71.0 ka BP and ca. 9.0 ka cal BP in the ARO 06 01 core. PC1 and PC2 data are from previous research [32] and represent the long-term background fluxes of inorganic particulate material and the delivery of large amounts of terrigenous particles transported during wet events, respectively. The $\delta^{13}C$ (‰) general trend indicates C_3 and C_4 vegetation dominance. Wet events according to $\delta^{13}C$ (‰) excursions and PC2 peaks that match with Hg concentration increases (blue bars); the dashed line indicates the position of the $\delta^{13}C$ (‰) excursion in agreement with the literature (see text). A red discontinuous bar indicates a highly oxidized peat section. Discontinuous trend lines indicate sections with chronological uncertainty. Cold periods are indicated (*).

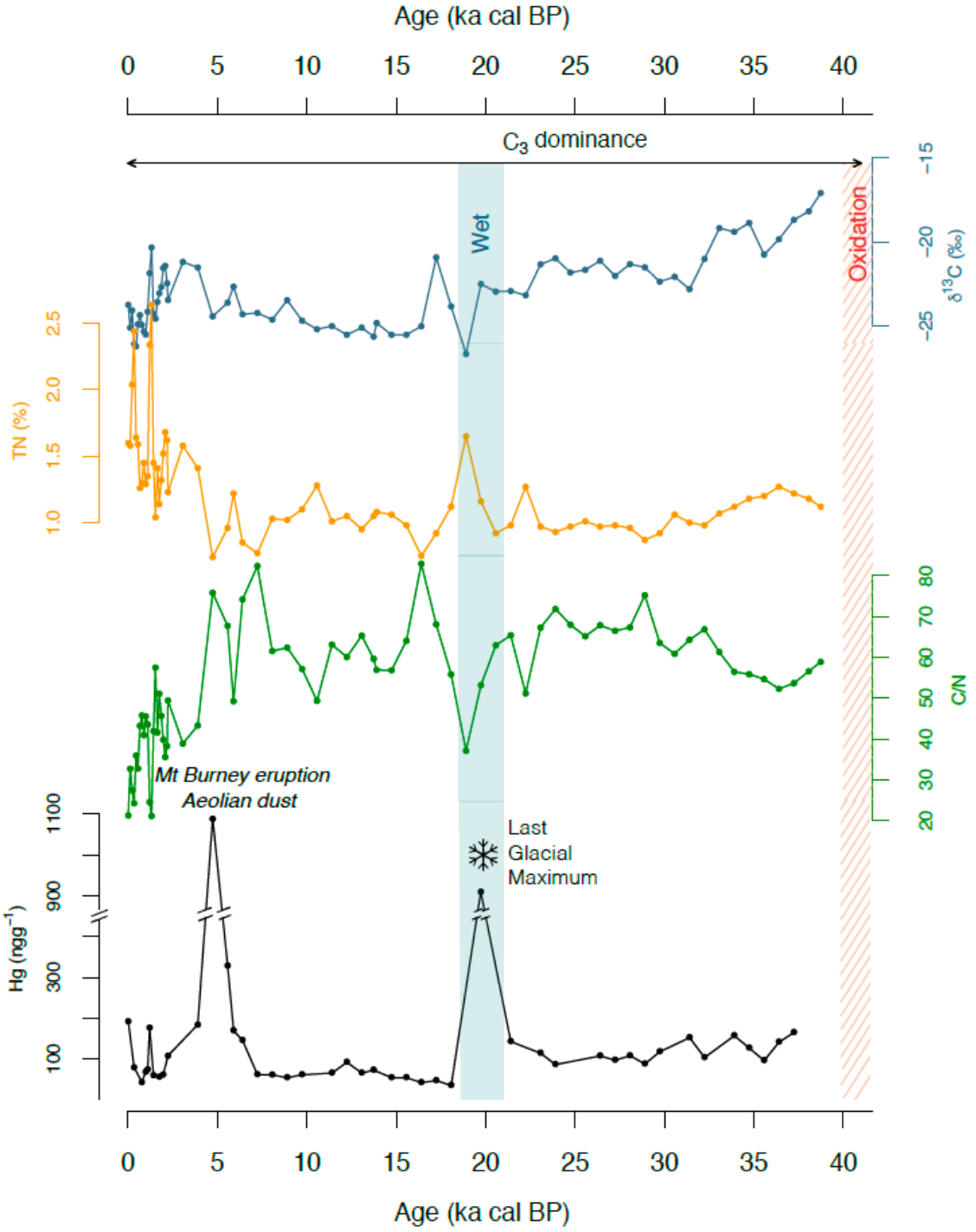

Figure 5. Mercury concentration and main proxies uses to reconstruct the environment in Rano Aroi in the last ca. 39.0 ka cal BP in the ARO 08 02 core; from bottom to top: Hg concentration, C/N, TN and δ^{13}C) [32]. Wet events according to δ^{13}C (‰) excursions that match with Hg concentration increases (blue bars); the dashed line indicates the position of the δ^{13}C (‰) excursion in agreement with the literature (see text). Cold periods are indicated (*).

Maxima Hg values in the Pleistocene and Holocene sections of Rano Aroi are comparatively high with respect to other peatlands worldwide, even in sections affected by anthropogenic emissions. For example, for the Industrial Period, maxima of ~800 ng g^{-1} were reported for the Czech Republic [45], >400 ng g^{-1} for Scotland [46,47], ca. 600 ng g^{-1} in Northeast China [48], ca. 130 ng g^{-1} for Canada [49], and ca. 300 ng g^{-1} in Spain [43]. Our two maxima of natural Hg concentrations

are, however, similar to those (up to 1100 ng g^{-1}) found in four peat cores from Belgium, dating to AD 1930–1980, which were interpreted to be associated with coal burning and smelter emissions [50]. Pre-Industrial Hg concentrations in the previously mentioned records are quite heterogeneous (such as 40–50 ng g^{-1} in the peatlands studied in the Czech Republic [45] or 111 ± 64 ng g^{-1} in the records from Northeast China [48]), but are in the range of the ARO records. These comparisons suggest that, under natural conditions, as expected in Easter Island at ~20 and ~4.7 ka cal BP, large amounts of Hg can accumulate over relatively low background values.

4.2. Environmental Conditions in Rano Aroi and Related Proxies

In previous studies on Rano Aroi cores, a combination of proxies was used to improve the knowledge on tropical and subtropical peat dynamics and the climatic history of Easter Island. The peatland demonstrated itself to be a good archive for reconstructing the environmental history of the area, which was mainly driven by climate [31,32], although without ruling out the effect of human activity in the last few millennia [51].

The $\delta^{13}C$ variations indicated two main climatic periods [31,32]. From ~70 to ~55 ka BP, high $\delta^{13}C$ values (mean −15‰, C_4-type plant remains) suggest the predominance of drier-colder climatic conditions, while from ~47 to ~8.5 ka cal BP low $\delta^{13}C$ values (−26 ‰, C_3-type plant remains) indicate a general dominance of wetter climate conditions (Figure 4). A gradual transition between both climates took place between ~55 ka BP and ~47 ka cal BP, and this is reflected by progressively lighter values of $\delta^{13}C$ (Figure 4). ARO 08 02 does not show this transition (Figure 5) because it only covers the last ~38 ka cal BP, but the $\delta^{13}C$ values shifted to lower values in agreement with the ARO 06 01 tendency. The long-term $\delta^{13}C$ trend was interrupted by negative excursions, interpreted as short wetter periods.

The same general pattern of $\delta^{13}C$ data is followed by PC1, the first component of a Principal Component Analysis performed on the inorganic fraction of Rano Aroi [32]. PC1 is characterized by large positive loadings (>0.7) of typically lithogenic elements and some metals. This component was identified as a proxy of the long-term fluxes of inorganic particulate material to the peatland. Its similarity with the $\delta^{13}C$ background trend suggests higher erosion during drier periods (~70 to ~55 ka BP)—probably due to lower vegetation cover—and an increasing mineral input during the short rainfall events previously mentioned (Figure 4). Another process, identified by the second component (PC2), is the occurrence of enhanced precipitation events related to the strong runoff and delivery of large amounts of terrigenous particles (probably rich in organic matter) from the soils of the catchment to the mire. Matching with these events, the C/N ratio and total nitrogen (TN) values show abrupt decreases and increases, respectively. Higher TN values and lower C/N ratio were attributed to a higher contribution of lacustrine algal material, in contrast to high C/N values that indicate higher proportions of terrestrial or aquatic plant (versus algae) organic matter [32].

4.3. Processes Controlling Hg Content

4.3.1. Climate

Temperature

Temperature has a significant effect on Hg oxidation. Atmospheric oxidation is currently thought to occur through a two-step oxidation mechanism, favored at cold temperatures, and based on an initial recombination of Hg(0) and Br followed by the addition of a second radical (e.g., Br, I, Cl, BrO, ClO, OH, NO_2 or HO_2) [4,52] in competition with the thermal dissociation of the HgBr intermediate [53]. Low temperatures stabilize the intermediate HgBr species, allowing the second oxidation step that yields divalent Hg to occur. As a result, the oxidation, and associated surface deposition, of Hg is accelerated during cold periods. The ~20 ka cal BP Hg maximum corresponds to the coldest phase, which occurred at the end of the Last Glacial Maximum [32]. Furthermore, the early Holocene Hg peak recorded in Aroi at ~8.5 ka cal BP (ARO 06 01) coincided with an unusual cold period known

as the 8.2 cooling event [54], given chronological uncertainties in the Aroi age-depth model [31]. Thus, the abrupt temperature shifts may have played a significant role in the Hg concentrations at the end of the LGM and the early Holocene. Similarly, at the time of the cold event Henrich 1 (H1, ~17.5), Hg content in Pinheiros reached the maxima [29]. None of the four identified processes controlling Hg content in Pinheiros mire (i.e., wet deposition, aeolian dust, catchment soil erosion and OM decomposition) were able to explain the peak of Hg during H1 [29]. However, the results obtained in Rano Aroi suggest that the increase during the H1 was at least partially due to surface deposition associated with Hg atmospheric oxidation under cold conditions.

Effective Moisture

Increases in Hg concentration seem to match, at least partially, with strong runoff events, based on PC2 scores peaks (Figure 4). Six of these main events (centered at ~60.5, ~56.6 ka BP and ~46.5, ~43.5, ~20.0 and ~10.0 ka cal BP) coincide with peaks in Hg concentration, while PC2 peaks centered at ~54.0 and ~49.5 ka cal BP do not show correspondence with Hg rises (Figure 4). The PC2 peak at ~10 ka cal BP agrees also with an increase in Hg (333 ng g^{-1}) in ARO 06 01.

Increased rainfall, which is the main driver for runoff events, should be the common link with Hg rises in Rano Aroi through enhanced Hg-wet deposition. However, it is unclear whether this is the only mechanism controlling the increase in Hg concentration in peat during wetter periods, or whether other mechanisms like the catchment erosion effect, the mire vegetation, peat decomposition and volcanic activity may have played a role.

Dry vs. Wet Deposition in Rano Aroi

The oxidation and deposition of Hg from the atmosphere through rainfall is a well-known process in the Hg cycle, however the importance of this process in environmental records is still under debate. Mercury isotopic analyses in living sphagnum mosses, upper peat layers, and rainwater samples were used in a recent publication to investigate the dominant modern Hg depositional processes in peat bogs [55]. The results of the three-year field experiment indicated that Hg deposition was dominated by gaseous elemental Hg dry deposition (79%) rather than wet deposition (21%). However, a later paleolimnological study conducted in a Pyrenean lake [24] showed that increased precipitation and more humid conditions controlled Hg accumulation in the area at a centennial scale, suggesting that wet deposition was the main driver at longer time-scales. In the tropical Pacific, modeling exercises during the pre-industrial period suggest dry deposition of Hg(II) as the main process governing Hg accumulation onto the land surface, with approximate values of ~4–5 μg m^{-2} $year^{-1}$ Hg(II) dry deposition in the Easter Island region [56]. Therefore, dry deposition may explain background Hg values in Rano Aroi. Nevertheless, other physico-chemical factors may also be considered when interpreting the interplay between dry and wet deposition onto land surfaces (i.e., peatlands and lakes). Large uncertainties exist regarding the atmospheric reduction of newly formed oxidized Hg(II). Although clouds enhance the scavenging and deposition of Hg to the surface, cloud droplets have also been suggested to be the medium where Hg(II) is reduced to elemental Hg, which is then re-emitted back to the gas phase [57]. Therefore, in the presence of clouds during rainy periods the dry deposition of atmospheric Hg may be slowed down. This would compete with wet deposition of Hg via precipitation, although it is almost certain that the latter would dominate the overall net atmospheric deposition of Hg to the surface. Thus, variable cloudiness might partially explain the discrepancies between the Pyrenean records.

At the Pleistocene scale, evidence supports the role of rainfall in intensifying Hg deposition. In Pinheiros mire, higher Hg concentrations found during a humid period from ~26.7 to ~2.8 ka cal BP were interpreted to result from increases in Hg concentration driven by precipitation (wet deposition—rainfall) [29].

Several differences exist in the Rano Aroi Hg cycle with respect to Pinheiros. First, the increases in Hg concentration are related to abrupt rainfall events (throughout ARO 08 02 and ARO 06 01) instead

of being a continuous process over a long time period. Second, there is apparently no dilution effect, due to the input of inorganic matter from the catchment despite the increased delivery of terrigenous material to the peatland during high-rainfall episodes [32]. Third, considering the extraordinary Hg peaks in the Rano Aroi cores (~1000 ng g^{-1}), there is a wider range in Hg concentrations than in Pinheiros (36–370 ng g^{-1}). This difference may be due to the high interannual rainfall variability in Easter Island (from 500–1800 mm), or indicate that other processes may have played a role in Hg deposition or accumulation.

The good match between the increases in Hg during wet periods in the mentioned long-term records suggests that Hg wash out from the atmosphere and deposition should be the main driver. In spite of dry deposition being found to be the main mechanism in the three-year study of the French bogs [55], it is possible that the perspective provided by the Pleistocene records (as Rano Aroi and Pinheiros) might highlight the dominance of the longer-term wet deposition processes (Figure 6).

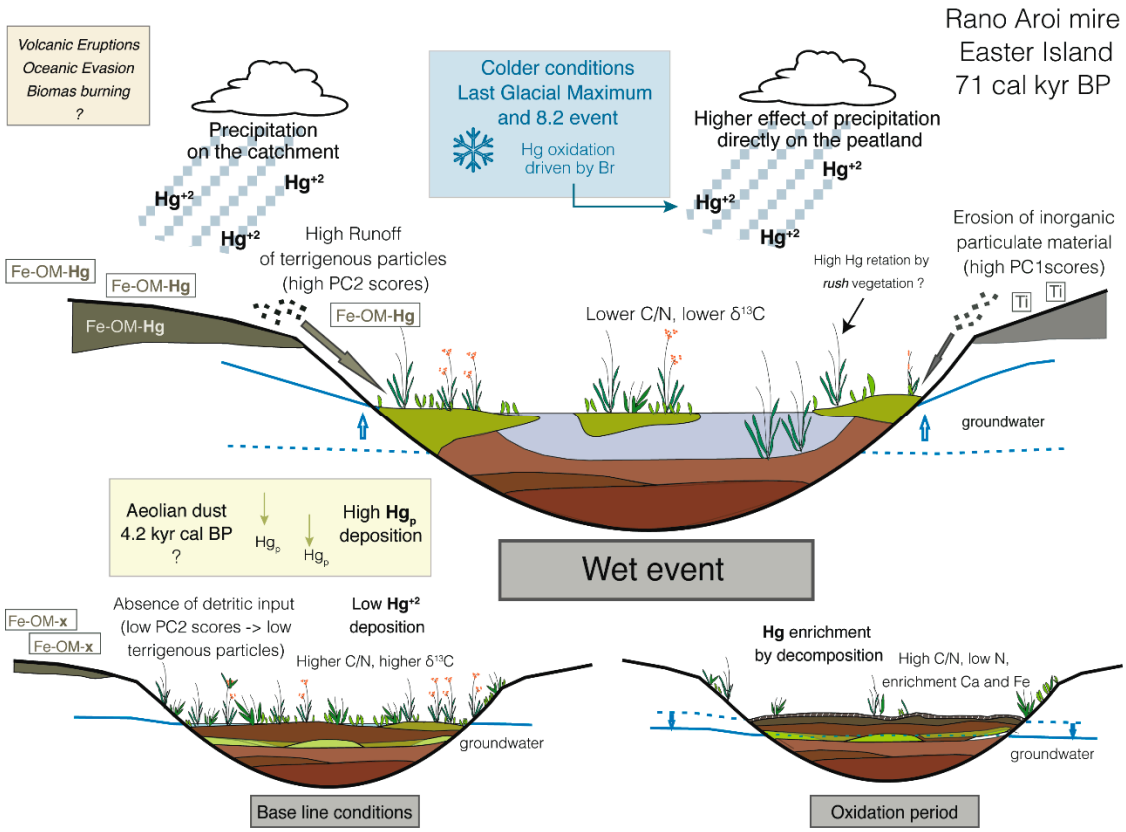

Figure 6. Mire schematic model indicating the processes controlling Hg deposition and accumulation under different environmental conditions. During rainfall events, Hg accumulates via wet deposition directly to the mire or through catchment soils. In baseline conditions the Hg accumulation is low. Under the dry peatland stage (i.e., ca. 40.0–42.0 ka cal BP) the peat-organic matter decomposition increases Hg content. The effect of vegetation and volcanic activity is not well addressed in this study. Modified from previous research [31].

4.3.2. Effect of Catchment Erosion: Geologic Materials and Catchment Soils

The direct contribution of local geologic materials to Hg concentration in the peat during high-rainfall events is negligible. The small catchment (15.82 km^2) is composed of highly porphyritic olivinic tholeite and basalt and hawaiite lava flows [34]. Specific information for Hg in basaltic materials is sparse in the published scientific literature. The most recent reviews of available data indicate that Hg in basalts is variable, generally in the range of 2–35 ng g^{-1} [58]. Data from basaltic reference materials showed that the Hg content in samples from island arcs or the circum-Pacific belt

is lower than that of samples from the continental origin, with concentrations generally at the lower end of the mean for the basaltic samples analyzed (7–34 ng g^{-1}) [59]. According to this, we would expect a low contribution of Hg from the catchment materials due to weathering.

However, catchment soils may maximize the effect of increased Hg concentration during rainfall events. Volcanic soils can retain Hg released form the parent material, as well as that deposited from the atmospheric pool [60]. As mentioned above, the type of geological material in the Rano Aroi catchment does not seem to have significant amounts of Hg so, most probably, all the Hg retained in the soils may ultimately originate from atmospheric deposition. The mobilization of Hg due to soil erosion [61] could also take place in volcanic areas, since Hg is associated with metal (Al-Fe)-humus complexes. Margalef et al. [31,32] also identified increases of Fe content and high values of PC2 (large positive loading of Fe) during enhanced rainfall periods. At least part of the Fe in (andic) volcanic soils may be as Fe-humus compounds [62], to which the Hg could be bound [60,63].These compounds may be transported to the mire by superficial runoff (Figure 6).

The comparison of Hg concentration in ARO 06 01 with the PC1 and PC2 components (the long-term background fluxes of inorganic particulate material and the delivery of large amounts of terrigenous particles, respectively) only shows agreement during the shorter wet events and not for the long-term trends (see Figure 4). This suggests that matter fluxes do not affect the concentration of Hg, but precipitation may be the common driver.

It is worth mentioning the presence of a short rise of Hg and PC2 in ARO 06 01 at ~37 ka cal BP that, according to the $\delta^{13}C$ record, does not correspond to a wet period (Figure 4), pointing to other processes as an increase of Hg concentration due to terrigenous Hg-rich input. However the existence of a chronological uncertainty in this section [32] invites caution in the interpretation.

The data support the idea that wet deposition—directly on the mire or through the catchment circuits—was the dominant process controlling Hg concentration in the Rano Aroi peatland since ~71.0 ka, essentially during high-rainfall events.

4.3.3. Other Processes: Mire Vegetation, Peat Decomposition, Aeolian Dust, Oceanic Evasion, and Volcanic Activity

The extremely high Hg concentration (1023 and 910 ng g^{-1} for ARO 06 01 and 08 02, respectively) at ~20 ka cal BP in both cores, and the Holocene major peaks at ~4.7 ka cal BP (ARO 08 02) and at ~8.5 ka cal BP (ARO 06 01), seem to have been caused by temperature and/or precipitation variability (that eventually control catchment erosion) since they coincide with colder periods with an increase of PC2 (higher run-off) and a decline in $\delta^{13}C$ (ARO 06 01 and ARO 08 02, respectively). For these peaks Hg is 3 and 4.5-fold (ARO 06 01 and 08 02, respectively) that of the next highest concentration (~300 ng g^{-1}), suggesting the short-lived nature of these Hg increase episodes, which could indicate other processes may have enhanced Hg concentration in the mire.

Mire Vegetation

It has been shown that vegetation type and degree of decomposition can affect the Hg content in peat [64]. Table 1 reveals that different vegetation present in the island may involve different Hg concentrations in plant remains. According to the data presented here (Table 1) an increase in the abundance of rush, which showed large (~11,000 ng g^{-1}) Hg concentrations, coupled with more humid conditions by ~20 ka cal BP, might help to explain these increases in Hg (Figure 6). However, we have no certainty of the presence of rush in the mire catchment at present, and the available pollen and macro remains data [31,32,65] do not allow us to support this speculation.

Peat Decomposition

The effect of organic matter decomposition in Hg accumulation is still a subject of debate. For short-term periods, it has been proposed that increased decomposition leads to an increase in Hg concentration [12,66]. This could be the situation during the extreme oxidation event caused by

the drought period which occurred at ~40.0 cal ka BP (Figure 4), when the Hg concentration slightly increased (Figures 4 and 6). On the other hand, the available data for longer Pleistocene-Holocene records, such as that of the Pinheiros mire [29], suggest that the effect of peat decomposition on Hg concentrations exponentially decreases to be almost negligible in peats with ages older than 10–11 ka [29]. There is no general decomposition trend in Rano Aroi and the short-term changes (reflected by changes in C/N ratio) seem to respond to enhanced rainfall periods and associated changes in mire vegetation [31], that may not have affected the Hg concentrations.

Aeolian Dust

Wind-borne dust particles derived from remote sources with higher Hg concentrations may also constitute a plausible explanation for the Hg peaks in the Aroi sedimentary sequence. Enhanced atmospheric dust deposition during the LGM may have also controlled the increase in Hg concentration in Aroi at 20 ka BP. This effect has been recently shown [28] to explain the high Hg accumulation rates in Caço lake (NE Brazil) between ~20 and 17 ka BP. LGM atmospheric elevated dust loadings in the Southern Hemisphere had a most likely source area in the Australian region, where increased aridity and less-efficient scavenging during this period would have enhanced Hg-enriched wind-born particles transported by westerlies to the South Pacific ocean [67]. Similarly, dust deposition together with cold conditions were suggested to be the cause of the increase of Hg during the 8.2 event in the Pinheiros mire record [29].

The mid-Holocene Hg peak in the Aroi peat record is also in agreement with the maximum Hg accumulation recorded at 4.2 ka cal BP in varved Elk Lake (North America) [68]. These authors found a causative factor between increased aeolian dust transport and deposition from remote locations with Hg-enriched soils. This period recorded a severe aridification at a global scale [69] that might have increased dust fluxes and transport in a similar pattern as during the LGM. Thus, Hg depositional patterns may have varied following aeolian dust fluxes from remote locations, demonstrating the significance of Hg bound to mineral particles in the Hg load in terrestrial ecosystems.

Oceanic Evasion

Biologically productive regions in the tropical Pacific Ocean are a significant source of atmospheric Hg, mainly relating to phytoplankton's conversion of seawater Hg(II) to Hg(0) [70]. Evasion of Hg from surface ocean Pacific waters in the region is further supported by results that account for oceanic evasion fluxes of 4–5 $\times$ 10^{-6} g m^{-2} $year^{-1}$ in oceanic areas near Easter Island, based on the modeling of the Pre-Industrial period [56]. During the LGM, a three-fold increase in Hg concentration in Dome C in Antarctica was attributed to higher oceanic productivity [71] increasing Hg emissions to the atmosphere and further deposition. However, Hg peaks in the Rano Aroi did not occur during periods of major oceanic productivity in the equatorial and tropical Pacific [72,73]. Thus, oceanic productivity will most likely have a significant contribution to the background Hg levels measured in the Aroi peat record.

Volcanic Activity

Individual volcanic eruptions have been identified for a long time as important natural sources of Hg. In addition to the direct emission of Hg, mainly as Hg(0) species [74,75], volcanic activity can increase the deposition of Hg to the environment by the oxidation of Hg(0) to Hg(II) [76]. The co-emission of Hg(0) and Br and SO_2 in volcanic plumes leads to an increase of Hg(II) formation that can easily be scavenged from the atmosphere by precipitation [76]. Furthermore, as the background atmospheric Hg is affected by the plume chemistry, the background Hg concentrations would be triggered by this mechanism and the total Hg deposit will be higher [76]. Thus, volcanic activity should also be considered in order to understand the triggers of the short-lived Hg peaks in Easter Island. Despite there being no volcanic lava flows older than two or three thousand years from Terevaka (one of the main volcanic structures in the island) [77], the Rano Aroi cores do not show evidence

of recent volcanic activity (i.e., tephra layers). The absence of recorded volcanic eruptions on the island does not rule out the possibility of Hg degassing or Hg depletion by plume chemistry by active fumaroles, especially on an island containing more than 70 volcano craters [33,34]. Data (tephra layers) from South Patagonia indicated volcanic eruptions at ~4.2 ka cal BP and ~7.7 ka cal BP, identified as the Mt Burney (52° S 72° W) and Hudson volcanic eruptions (45° S 72° W), respectively [78,79]. We have no data to support the effect of these volcanic events for the Hg peak at ~4.7 ka cal BP (ARO 08 02) and/or at ~8.5 ka cal BP (ARO 06 01) in Easter Island, but they cannot be discarded as a possible Hg source. Moreover, although there is some mismatch between the Hg peak and the Hudson volcanic eruption, it has been shown that this specific eruption (at ~7.7 ka cal BP) modified the atmospheric deposition dust during a period of ~700 years [80]. A higher resolution would be needed in this section of the cores, as well as more cores, to confirm the hypothesis of the effect of volcanism and differences in intensity (i.e., differences in Hg concentration) between both events.

Fire Regime

Biomass burning is an important source of Hg emissions to the atmosphere [81]. Although Hg(0) represents the greatest fraction of Hg from biomass burning, modeling studies have shown that Hg(p) (with a shorter life-span in the atmosphere) also represent a significant amount of the Hg released during fire episodes [82]. Thus, we cannot exclude the effect of fire regimes to explain the short-nature Hg peaks through increasing atmospheric Hg concentration. For example during the LGM, charcoal data indicates an increase in fire activity at the tropical latitudes of South America [83]. What might have been an extra Hg emission to the atmosphere, was then eventually deposited at Easter Island during heavy rainfall episodes.

5. Conclusions

The Hg record in the Rano Aroi cores shows a huge range of values between 35–1000 ng g^{-1}, mostly driven by wet precipitation—directly on the mire or through the catchment circuits—essentially during high-rainfall events. Two large maxima occurred at the end of the LGM (~20 ka cal BP) and at ~8.5 ka cal BP, both periods of general cold climatic conditions and wetness in Rano Aroi. Low temperature would accelerate the atmospheric oxidation of Hg(0) to divalent Hg, and if combined with high precipitation this would result in very efficient surface deposition of atmospheric Hg. Thus, both colder and humid conditions would have favored Hg accumulation in Rano Aroi, since Hg deposition is controlled by temperature and humidity variations [14,24].

Other processes such as mire vegetation, peat decomposition, aeolian dust, oceanic evasion, and volcanic activity (direct Hg emission and Hg oxidation) may have played a secondary role in Hg content. Oceanic evasion might have played a role as a general background Hg source, and increases in the fire regimen during the LGM at the tropical latitudes of South America might have been an extra Hg emission to the atmosphere that was eventually deposited on Easter Island during heavy rainfall episodes. Moreover, wind-borne dust particles derived from remote sources with higher Hg concentrations might also play a role in enhanced Hg concentrations during the LGM, and especially during the mid-Holocene Hg peak (4.2 ka cal BP), in agreement with previous works.

The combinations of these processes cause a range of variation of Hg concentrations of 28-fold in a remote and undisturbed area, at least during the studied period. The maximum values are higher than those recorded in most peat records belonging to the Industrial Period, highlighting that natural factors played a significant role in local Hg accumulation—sometimes even more so than anthropogenic sources.

Author Contributions: Data curation, M.P.-R. and O.M.; Formal analysis, M.P.-R. and O.M.; Funding acquisition, S.P.-R., S.G. and A.M.C.; Investigation, M.P.-R. and A.M.C.; Project administration, S.P.-R., S.G. and A.M.C.; Supervision, A.M.C.; Writing—original draft, M.P.-R.; Writing—review & editing, M.P.-R., O.M., J.P.C., A.S.-L., S.P.-R., S.G. and A.M.C.

Funding: This research was funded by the Spanish Ministry of Science and Education through the projects LAVOLTER [CGL2004-00683/BTE], GEOBILA [CGL2007-60932/BTE], R2014/001 and GPC GI-1553 [Dirección Xeral I+D, Xunta de Galicia].

Acknowledgments: We would like to thank CONAF (Chile) and the Rirorokо family for the facilities provided on Easter Island and Jesús R. Aboal (Universidade de Santiago de Compostela) for laboratory facilities.

Conflicts of Interest: The authors declare that the research was conducted in the absence of any commercial or financial relationships that could be construed as a potential conflict of interest.

References

1. Schroeder, W.H.; Munthe, J. Atmospheric mercury—An overview. *Atmos. Environ.* **1998**, *32*, 809–822. [CrossRef]
2. Hylander, L.D.; Meili, M. The Rise and Fall of Mercury: Converting a Resource to Refuse After 500 Years of Mining and Pollution. *Crit. Rev. Environ. Sci. Technol.* **2005**, *35*, 1–36. [CrossRef]
3. Horowitz, H.M.; Jacob, D.J.; Amos, H.M.; Streets, D.G.; Sunderland, E.M. Historical mercury releases from commercial products: Global environmental implications. *Environ. Sci. Technol.* **2014**, *48*, 10242–10250. [CrossRef] [PubMed]
4. Wang, F.; Saiz-Lopez, A.; Mahajan, A.S.; Gómez Martín, J.C.; Armstrong, D.; Lemes, M.; Hay, T.; Prados-Roman, C. Enhanced production of oxidised mercury over the tropical Pacific Ocean: A key missing oxidation pathway. *Atmos. Chem. Phys.* **2014**, *14*, 1323–1335. [CrossRef]
5. Fitzgerald, W.F.; Mason, R.P. The global mercury cycle: Oceanic and anthropogenic aspects. In *Global and Regional Mercury Cycles: Sources, Fluxes and Mass Balances*; Springer: Berlin/Heidelberg, Germany, 1996; pp. 85–108.
6. Amos, H.M.; Sonke, J.E.; Obrist, D.; Robins, N.; Hagan, N.; Horowitz, H.M.; Mason, R.P.; Witt, M.; Hedgecock, I.M.; Corbitt, E.S.; et al. Observational and modeling constraints on global anthropogenic enrichment of mercury. *Environ. Sci. Technol.* **2015**, *49*, 4036–4047. [CrossRef] [PubMed]
7. Biester, H.; Bindler, R.; Martinez-Cortizas, A.; Engstrom, D.R. Modeling the Past Atmospheric Deposition of Mercury Using Natural Archives. *Environ. Sci. Technol.* **2007**, *41*, 4851–4860. [CrossRef] [PubMed]
8. Engstrom, D.R.; Fitzgerald, W.F.; Cooke, C.A.; Lamborg, C.H.; Drevnick, P.E.; Swain, E.B.; Balogh, S.J.; Balcom, P.H. Atmospheric Hg emissions from preindustrial gold and silver extraction in the Americas: A reevaluation from lake-sediment archives. *Environ. Sci. Technol.* **2014**, *48*, 6533–6543. [CrossRef] [PubMed]
9. Cloy, J.M.; Farmer, J.G.; Graham, M.C.; MacKenzie, A.B.; Cook, G.T. Historical records of atmospheric Pb deposition in four Scottish ombrotrophic peat bogs: An isotopic comparison with other records from western Europe and Greenland. *Glob. Biogeochem. Cycles* **2008**, *22*. [CrossRef]
10. Zaferani, S.; Pérez-Rodríguez, M.; Biester, H. Diatom ooze—A large marine mercury sink. *Science* **2018**, eaat2735. [CrossRef] [PubMed]
11. Lamborg, C.H.; Fitzgerald, W.F.; Damman, A.W.H.; Benoit, J.M.; Balcom, P.H.; Engstrom, D.R. Modern and historic atmospheric mercury fluxes in both hemispheres: Global and regional mercury cycling implications. *Glob. Biogeochem. Cycles* **2002**, *16*, 1104. [CrossRef]
12. Biester, H.; Martinez-Cortizas, A.; Birkenstock, S.; Kilian, R. Effect of Peat Decomposition and Mass Loss on Historic Mercury Records in Peat Bogs from Patagonia. *Environ. Sci. Technol.* **2003**, *37*, 32–39. [CrossRef] [PubMed]
13. Biester, H.; Keppler, F.; Putschew, A.; Martinez-Cortizas, A.; Petri, M. Halogen Retention, Organohalogens, and the Role of Organic Matter Decomposition on Halogen Enrichment in Two Chilean Peat Bogs. *Environ. Sci. Technol.* **2004**, *38*, 1984–1991. [CrossRef] [PubMed]
14. Martínez Cortizas, A.; Pontevedra-Pombal, X.; García-Rodeja, E.; Nóvoa-Muñoz, J.C.; Shotyk, W. Mercury in a Spanish Peat Bog: Archive of Climate Change and Atmospheric Metal Deposition. *Science* **1999**, *284*, 939–942. [CrossRef] [PubMed]
15. Jitaru, P.; Gabrielli, P.; Marteel, A.; Plane, J.M.C.; Planchon, F.A.M.; Gauchard, P.-A.; Ferrari, C.P.; Boutron, C.F.; Adams, F.C.; Hong, S.; et al. Atmospheric depletion of mercury over Antarctica during glacial periods. *Nat. Geosci.* **2009**, *2*, 505–508. [CrossRef]

16. Outridge, P.M.; Sanei, H.; Stern, G.A.; Hamilton, P.B.; Goodarzi, F. Evidence for control of mercury accumulation rates in Canadian High Arctic Lake sediments by variations of aquatic primary productivity. *Environ. Sci. Technol.* **2007**, *41*, 5259–5265. [CrossRef] [PubMed]
17. Kirk, J.L.; Muir, D.C.M.; Antoniades, D.; Douglas, M.S.V.; Evans, M.S.; Jackson, T.A.; Kling, H.; Amoureux, S.; Lim, D.S.S.; Pienitz, R.; et al. Climate change and mercury accumulation in canadian high and subarctic lakes. *Environ. Sci. Technol.* **2011**, *45*, 964–970. [CrossRef] [PubMed]
18. Biester, H.; Pérez-Rodríguez, M.; Gilfedder, B.-S.; Martínez Cortizas, A.; Hermanns, Y.-M. Solar irradiance and primary productivity controlled mercury accumulation in sediments of a remote lake in the Southern Hemisphere during the past 4000 years: Primary productivity and mercury accumulation. *Limnol. Oceanogr.* **2018**, *63*, 540–549. [CrossRef]
19. Rydberg, J.; Klaminder, J.; Rosén, P.; Bindler, R. Climate driven release of carbon and mercury from permafrost mires increases mercury loading to sub-arctic lakes. *Sci. Total Environ.* **2010**, *408*, 4778–4783. [CrossRef] [PubMed]
20. Ribeiro Guevara, S.; Meili, M.; Rizzo, A.; Daga, R.; Arribére, M. Sediment records of highly variable mercury inputs to mountain lakes in Patagonia during the past millennium. *Atmos. Chem. Phys.* **2010**, *10*, 3443–3453. [CrossRef]
21. Daga, R.; Ribeiro Guevara, S.; Pavlin, M.; Rizzo, A.; Lojen, S.; Vreča, P.; Horvat, M.; Arribére, M. Historical records of mercury in southern latitudes over 1600 years: Lake Futalaufquen, Northern Patagonia. *Sci. Total Environ.* **2016**, *553*, 541–550. [CrossRef] [PubMed]
22. Roos-Barraclough, F.; Martinez-Cortizas, A.; García-Rodeja, E.; Shotyk, W.; García-Rodeja, E.; Shotyk, W. A 14,500 year record of the accumulation of atmospheric mercury in peat: Volcanic signals, anthropogenic influences and a correlation to bromine accumulation. *Earth Planet. Sci. Lett.* **2002**, *202*, 435–451. [CrossRef]
23. Schuster, P.F.; Krabbenhoft, D.P.; Naftz, D.L.; Cecil, L.D.; Olson, M.L.; Dewild, J.F.; Susong, D.D.; Green, J.R.; Abbott, M.L. Atmospheric Mercury Deposition during the Last 270 Years: A Glacial Ice Core Record of Natural and Anthropogenic Sources. *Environ. Sci. Technol.* **2002**, *36*, 2303–2310. [CrossRef] [PubMed]
24. Corella, J.P.; Wang, F.; Cuevas, C.A. 700 years reconstruction of mercury and lead atmospheric deposition in the Pyrenees (NE Spain). *Atmos. Environ.* **2017**, *155*, 97–107. [CrossRef]
25. Hermanns, Y.; Biester, H. Anthropogenic mercury signals in lake sediments from southernmost Patagonia, Chile. *Sci. Total Environ.* **2013**, *445–446*, 126–135. [CrossRef] [PubMed]
26. Hermanns, Y.-M.; Cortizas, A.M.; Arz, H.; Stein, R.; Biester, H. Untangling the influence of in-lake productivity and terrestrial organic matter flux on 4250 years of mercury accumulation in Lake Hambre, Southern Chile. *J. Paleolimnol.* **2012**, *49*, 563–573. [CrossRef]
27. Franzen, C.; Kilian, R.; Biester, H. Natural mercury enrichment in a minerogenic fen–evaluation of sources and processes. *J. Environ. Monit.* **2004**, *6*, 466–472. [CrossRef] [PubMed]
28. De Lacerda, L.D.; Turcq, B.; Sifeddine, A.; Cordeiro, R.C. Mercury accumulation rates in Caço Lake, NE Brazil during the past 20,000 years. *J. S. Am. Earth Sci.* **2017**, *77*, 42–50. [CrossRef]
29. Pérez-Rodríguez, M.; Horák-Terra, I.; Rodríguez-Lado, L.; Aboal, J.R.; Martínez Cortizas, A. Long-Term (~57 ka) controls on mercury accumulation in the souther hemisphere reconstructed using a peat record from pinheiro mire (Minas Gerais, Brazil). *Environ. Sci. Technol.* **2015**, *49*, 1356–1364. [CrossRef] [PubMed]
30. Pérez-Rodríguez, M.; Horák-Terra, I.; Rodríguez-Lado, L.; Martínez Cortizas, A. Modelling mercury accumulation in minerogenic peat combining FTIR-ATR spectroscopy and partial least squares (PLS). *Spectrochim. Acta Part A Mol. Biomol. Spectrosc.* **2016**, *168*, 65–72. [CrossRef] [PubMed]
31. Margalef, O.; Cañellas-Boltà, N.; Pla-rabes, S.; Giralt, S.; Pueyo, J.J.; Joosten, H.; Rull, V.; Buchaca, T.; Hernández, A.; Valero-Garcés, B.L.; et al. 70,000 year multiproxy record of climatic and environmental change from Rano Aroi peatland (Easter Island). *Glob. Planet. Chang.* **2013**, *108*, 72–84. [CrossRef]
32. Margalef, O.; Martínez Cortizas, A.; Kylander, M.; Pla-Rabes, S.; Cañellas-Boltà, N.; Pueyo, J.J.; Sáez, A.; Valero-Garcés, B.L.; Giralt, S. Environmental processes in Rano Aroi (Easter Island) peat geochemistry forced by climate variability during the last 70 kyr. *Palaeogeogr. Palaeoclimatol. Palaeoecol.* **2014**, *414*, 438–450. [CrossRef]
33. Baker, P.E.; Buckley, F.; Holland, J.G. Petrology and geochemistry of Easter Island. *Contrib. Mineral. Petrol.* **1974**, *44*, 85–100. [CrossRef]
34. González-Ferrán, O.; Mazzuoli, R.; Lahsen, A. *Geología del Complejo Volcánico Isla de Pascua, Rapa Nui, Chile: V Region-Valparaiso*; Centro de Estudio Volcanológicos de Santiago: Santiago, Chile, 2004.

35. Sáez, A.; Valero-Garcés, B.L.; Giralt, S.; Moreno, A.; Bao, R.; Pueyo, J.J.; Hernández, A.; Casas, D. Glacial to Holocene climate changes in the SE Pacific. The Raraku Lake sedimentary record (Easter Island, 27 S). *Q. Sci. Rev.* **2009**, *28*, 2743–2759. [CrossRef]
36. Junk, C.; Claussen, M. Simulated climate variability in the region of Rapa Nui during the last millennium. *Clim. Past* **2011**, *7*, 579–586. [CrossRef]
37. Zizka, G. Flowering plants of Easter Island. In *Palmarum Hortus Francofurtensis*; Palmengarten: Frankfurt am Main, Germany, 1991.
38. Flenley, J.R.; King, S.M. Late Quaternary pollen records from Easter Island. *Nature* **1984**, *307*, 47–50. [CrossRef]
39. Flenley, J.R.; King, A.S.M.; Jackson, J.; Chew, C.; Teller, J.T.; Prentice, M.E. The Late Quaternary vegetational and climatic history of Easter Island. *J. Quat. Sci.* **1991**, *6*, 85–115. [CrossRef]
40. Reimer, P.J.; Baillie, M.G.L.; Bard, E.; Bayliss, A.; Beck, J.W.; Bertrand, C.J.H.; Blackwell, P.G.; Buck, C.E.; Burr, G.S.; Cutler, K.B. IntCal04 terrestrial radiocarbon age calibration, 0–26 cal kyr BP. *Radiocarbon* **2004**, *46*, 1029–1058. [CrossRef]
41. Danzeglocke, U.; Jöris, O.; Weninger, B. CalPal-2007. Available online: http://www.calpal-online.de (accessed on 3 May 2009).
42. Steinnes, E.; Rühling, Å.; Lippo, H.; Mäkinen, A. Reference materials for large-scale metal deposition surveys. *Accredit. Qual. Assur.* **1997**, *2*, 243–249. [CrossRef]
43. Martínez Cortizas, A.; Peiteado Varela, E.; Bindler, R.; Biester, H.; Cheburkin, A. Reconstructing historical Pb and Hg pollution in NW Spain using multiple cores from the Chao de Lamoso bog (Xistral Mountains). *Geochim. Cosmochim. Acta* **2012**, *82*, 68–78. [CrossRef]
44. Bindler, R.; Klarqvist, M.; Klaminder, J.; Förster, J. Does within-bog spatial variability of mercury and lead constrain reconstructions of absolute deposition rates from single peat records? The example of Store Mosse, Sweden. *Glob. Biogeochem. Cycles* **2004**, *18*, 1–12. [CrossRef]
45. Zuna, M.; Ettler, V.Š.O.; Mihaljevi, M.; Šebek, O.; Mihaljevič, M. Mercury accumulation in peatbogs at Czech sites with contrasting pollution histories. *Sci. Total Environ.* **2012**, *424*, 322–330. [CrossRef] [PubMed]
46. Farmer, J.G.; Anderson, P.; Cloy, J.M.; Graham, M.C.; MacKenzie, A.B.; Cook, G.T. Historical accumulation rates of mercury in four Scottish ombrotrophic peat bogs over the past 2000 years. *Sci. Total Environ.* **2009**, *407*, 5578–5588. [CrossRef] [PubMed]
47. Yang, H.; Rose, N.; Boyle, J.; Battarbee, R. Storage and distribution of trace metals and spheroidal carbonaceous particles (SCPs) from atmospheric deposition in the catchment peats of Lochnagar, Scotland. *Environ. Pollut.* **2001**, *115*, 231–238. [CrossRef]
48. Tang, S.; Huang, Z.; Liu, J.; Yang, Z.; Lin, Q. Atmospheric mercury deposition recorded in an ombrotrophic peat core from Xiaoxing'an Mountain, Northeast China. *Environ. Res.* **2012**, *118*, 145–148. [CrossRef] [PubMed]
49. Outridge, P.M.; Rausch, N.; Percival, J.B.; Shotyk, W.; McNeely, R. Comparison of mercury and zinc profiles in peat and lake sediment archives with historical changes in emissions from the Flin Flon metal smelter, Manitoba, Canada. *Sci. Total Environ.* **2011**, *409*, 548–563. [CrossRef] [PubMed]
50. Allan, M.; Le Roux, G.; Sonke, J.E.; Piotrowska, N.; Streel, M.; Fagel, N. Reconstructing historical atmospheric mercury deposition in Western Europe using: Misten peat bog cores, Belgium. *Sci. Total Environ.* **2013**, *442*, 290–301. [CrossRef] [PubMed]
51. Rull, V.; Cañellas-Boltà, N.; Margalef, O.; Sáez, A.; Pla-Rabes, S.; Giralt, S. Late Holocene vegetation dynamics and deforestation in Rano Aroi: Implications for Easter Island's ecological and cultural history. *Q. Sci. Rev.* **2015**, *126*, 219–226. [CrossRef]
52. Saiz-Lopez, A.; von Glasow, R. Reactive halogen chemistry in the troposphere. *Chem. Soc. Rev.* **2012**, *41*, 6448–6472. [CrossRef] [PubMed]
53. Goodsite, M.E.; Plane, J.M.C.; Skov, H. A Theoretical Study of the Oxidation of Hg0 to HgBr2 in the Troposphere. *Environ. Sci. Technol.* **2004**, *38*, 1772–1776. [CrossRef] [PubMed]
54. Alley, R.B.; Mayewski, P.A.; Sowers, T.; Stuiver, M.; Taylor, K.C.; Clark, P.A. Holocene climate variability: A prominent widespread event 8200 years ago. *Geology* **1997**, *25*, 483–486. [CrossRef]
55. Enrico, M.; Le Roux, G.; Marusczak, N.; Heimbürger, L.-E.; Claustres, A.; Fu, X.; Sun, R.; Sonke, J.E. Atmospheric Mercury Transfer to Peat Bogs Dominated by Gaseous Elemental Mercury Dry Deposition. *Environ. Sci. Technol.* **2016**, acs.est.5b06058. [CrossRef] [PubMed]

56. Selin, N.E.; Jacob, D.J.; Yantosca, R.M.; Strode, S.; Jaeglé, L.; Sunderland, E.M. Global 3-D land-ocean-atmosphere model for mercury: Present-day versus preindustrial cycles and anthropogenic enrichment factors for deposition. *Glob. Biogeochem. Cycles* **2008**, *22*, 1–13. [CrossRef]
57. Holmes, C.D.; Jacob, D.J.; Corbitt, E.S.; Mao, J.; Yang, X.; Talbot, R.; Slemr, F. Global atmospheric model for mercury including oxidation by bromine atoms. *Atmos. Chem. Phys.* **2010**, *10*, 12037–12057. [CrossRef]
58. Carlson, R.W. *The Mantle and Core: Treatise on Geochemistry*; Elsevier: Amsterdam, The Netherlands, 2005; Volume 2, ISBN 0080549012.
59. Flanagan, F.J.; Moore, R.; Aruscavage, P.J. Mercury in Geologic Reference Samples. *Geostand. Newsl.* **1982**, *6*, 25–46. [CrossRef]
60. Peña-Rodríguez, S.; Pontevedra-Pombal, X.; Fernández-Calviño, D.; Taboada, T.; Arias-Estévez, M.; Martínez-Cortizas, A.; Nóvoa-Muñoz, J.C.; García-Rodeja, E. Mercury content in volcanic soils across Europe and its relationship with soil properties. *J. Soils Sediments* **2012**, *12*, 542–555. [CrossRef]
61. Roulet, M.; Lucotte, M.; Saint-Aubin, A.; Tran, S.; Rheault, I.; Farella, N.; Dezencourt, J.; Passos, C.-J.S.; Soares, G.S.; Guimaraes, J.-R. The geochemistry of mercury in central Amazonian soils developed on the Alter-do-Chao formation of the lower Tapajos River Valley, Para state, Brazil. *Sci. Total Environ.* **1998**, *223*, 1–24. [CrossRef]
62. García-Rodeja, E.; Nóvoa, J.C.; Pontevedra, X.; Martínez-Cortizas, A.; Buurman, P. Aluminium fractionation of European volcanic soils by selective dissolution techniques. *Soils Volcan. Reg. Eur.* **2004**, *56*, 325–351. [CrossRef]
63. Nóvoa-Muñoz, J.C.; Pontevedra-Pombal, X.; Martínez-Cortizas, A.; García-Rodeja Gayoso, E. Mercury accumulation in upland acid forest ecosystems nearby a coal-fired power-plant in Southwest Europe (Galicia, NW Spain). *Sci. Total Environ.* **2008**, *394*, 303–312. [CrossRef] [PubMed]
64. Rydberg, J.; Karlsson, J.; Nyman, R.; Wanhatalo, I.; Näthe, K.; Bindler, R. Importance of vegetation type for mercury sequestration in the northern Swedish mire, Rödmossamyran. *Geochim. Cosmochim. Acta* **2010**, *74*, 7116–7126. [CrossRef]
65. Margalef, O. *The Last 70 Ky of Rano Aroi (Easter Island, 27 °S) Peat Record: New Insights for the Central Pacific Paleoclimatology*; Universitat de Barcelona: Barcelona, Spain, 2014.
66. Martínez Cortizas, A.; Biester, H.; Mighall, T.; Bindler, R. Climate-driven enrichment of pollutants in peatlands. *Biogeosciences* **2007**, *4*, 905–911. [CrossRef]
67. Hesse, P.P.; McTainsh, G.H. Last Glacial Maximum to Early Holocene Wind Strength in the Mid-latitudes of the Southern Hemisphere from Aeolian Dust in the Tasman Sea. *Quat. Res.* **1999**, *52*, 343–349. [CrossRef]
68. Cannon, W.F.; Dean, W.E.; Bullock, J.H. Effects of Holocene Climate Change on Mercury Deposition in Elk Lake, Minnesota: The Importance of Eolian Transport in the Mercury Cycle Effects of Holocene climate change on mercury deposition in Elk Lake, Minnesota: The importance of eolian transpor. *Geology* **2003**, *31*, 187–190. [CrossRef]
69. DeMenocal, P.B. Cultural Responses to Climate Change During the Late Holocene. *Science* **2001**, *292*, 667–673. [CrossRef] [PubMed]
70. Kim, J.P.; Fitzgerald, W.F. Sea-Air Partitioning of Mercury in the Equatorial Pacific Ocean. *Science* **1986**, *231*, 1131–1133. [CrossRef] [PubMed]
71. Vandal, G.M.; Fitzgerald, W.F.; Boutron, C.F.; Candelone, J.-P. Variations in mercury deposition to Antarctica over the past 34,000 years. *Nature* **1993**, *362*, 621–623. [CrossRef]
72. Salvatteci, R.; Gutierrez, D.; Sifeddine, A.; Ortlieb, L.; Druffel, E.; Boussafir, M.; Schneider, R. Centennial to millennial-scale changes in oxygenation and productivity in the Eastern Tropical South Pacific during the last 25,000 years. *Q. Sci. Rev.* **2016**, *131*, 102–117. [CrossRef]
73. Costa, K.M.; Jacobel, A.W.; McManus, J.F.; Anderson, R.F.; Winckler, G.; Thiagarajan, N. Productivity patterns in the Equatorial Pacific over the last 30,000 years. *Glob. Biogeochem. Cycles* **2017**, *31*, 1–16. [CrossRef]
74. Bagnato, E.; Aiuppa, A.; Parello, F.; Calabrese, S.; D'Alessandro, W.; Mather, T.A.; McGonigle, A.J.S.; Pyle, D.M.; Wängberg, I. Degassing of gaseous (elemental and reactive) and particulate mercury from Mount Etna volcano (Southern Italy). *Atmos. Environ.* **2007**, *41*, 7377–7388. [CrossRef]
75. Witt, M.L.I.; Mather, T.A.; Pyle, D.M.; Aiuppa, A.; Bagnato, E.; Tsanev, V.I. Mercury and halogen emissions from Masaya and Telica volcanoes, Nicaragua. *J. Geophys. Res.* **2008**, *113*, B6. [CrossRef]
76. Von Glasow, R. Atmospheric chemistry in volcanic plumes. *Proc. Natl. Acad. Sci. USA* **2010**, *107*, 6594–6599. [CrossRef] [PubMed]

77. Baker, P.E. Preliminary account of recent geological investigations on Easter Island. *Geol. Mag.* **1967**, *104*, 116–122. [CrossRef]
78. McCulloch, R.D.; Davies, S.J. Late-glacial and Holocene palaeoenvironmental change in the central Strait of Magellan, southern Patagonia. *Palaeogeogr. Palaeoclimatol. Palaeoecol.* **2001**, *173*, 143–173. [CrossRef]
79. Stern, C.R. Holocene tephrochronology record of large explosive eruptions in the southernmost Patagonian Andes. *Bull. Volcanol.* **2008**, *70*, 435–454. [CrossRef]
80. Vanneste, H.; De Vleeschouwer, F.; Bertrand, S.; Martínez-Cortizas, A.; Vanderstraeten, A.; Mattielli, N.; Coronato, A.; Piotrowska, N.; Jeandel, C.; Roux, G. Le Elevated dust deposition in Tierra del Fuego (Chile) resulting from Neoglacial Darwin Cordillera glacier fluctuations. *J. Quat. Sci.* **2016**, *31*, 713–722. [CrossRef]
81. De Simone, F.; Cinnirella, S.; Gencarelli, C.N.; Yang, X.; Hedgecock, I.M.; Pirrone, N. Model study of global mercury deposition from biomass burning. *Environ. Sci. Technol.* **2015**, *49*, 6712–6721. [CrossRef] [PubMed]
82. De Simone, F.; Artaxo, P.; Bencardino, M.; Cinnirella, S.; Carbone, F.; D'Amore, F.; Dommergue, A.; Bin Feng, X.; Gencarelli, C.N.; Hedgecock, I.M.; et al. Particulate-phase mercury emissions from biomass burning and impact on resulting deposition: A modelling assessment. *Atmos. Chem. Phys.* **2017**, *17*, 1881–1899. [CrossRef] [PubMed]
83. Power, M.J.; Marlon, J.; Ortiz, N.; Bartlein, P.J.; Harrison, S.P.; Mayle, F.E.; Ballouche, A.; Bradshaw, R.H.W.; Carcaillet, C.; Cordova, C.; et al. Changes in fire regimes since the last glacial maximum: An assessment based on a global synthesis and analysis of charcoal data. *Clim. Dyn.* **2008**, *30*, 887–907. [CrossRef]